Supporting Information for:

Unravelling the Fine Structure of Stacked Bipyridine diamine-derived C_3-Discotics as Determined by X–ray Diffraction, Quantum-Chemical Calculations, Fast-MAS NMR and CD Spectroscopy

Thorsten Metzroth,[a] Anke Hoffmann,[b] Rafael Martín-Rapún,[c] Maarten M. J. Smulders,[c] Koen Pieterse,[c] Anja R. A. Palmans,[c] Jef A. J. M. Vekemans,[c] E. W. Meijer,[c] Hans W. Spiess,[b] and Jürgen Gauss[a]

[a] Institut für Physikalische Chemie, Universität Mainz, D-55099 Mainz, Germany.
[b] Max-Planck-Institute for Polymer Research, Postfach 3148, D-55021 Mainz, Germany.
[c] Laboratory of Macromolecular and Organic Chemistry, Eindhoven University of Technology, P.O. Box 513, 5600 MB, Eindhoven, The Netherlands.

Table of Contents

1. Experimental section

X-Ray Diffraction. For all SAXD and WAXD measurements the crude product was filled in a Lindemann glass capillary (0.9 mm diameter). Aligned samples were obtained by shearing the material against the wall of the capillary at a temperature at which the product is fluid enough, typically 170 ºC. Small-angle X-ray diffraction (SAXD) measurements were made using an homemade setup at AMOLF with a rotating anode X-ray generator (Rigaku RUH300, 18 kW) equipped with two parabolic multilayer mirrors (Bruker, Karlsruhe), giving a highly parallel beam (divergence of about 0.025º) of monochromatic Cu Kα radiation (λ = 0.154 nm). The SAXD intensity was collected with a 2D gas-filled wire detector (Bruker Hi-Star). A semitransparent beam stop placed in front of the area detector allowed for monitoring of the intensity of the direct beam. The SAXD intensities were corrected by subtracting a background that was normalised to the acquisition time. An adapted Linkam THMS600 temperature-controlled system was employed as the sample stage. To minimise the background signal, the glass windows in the sample stage were left out for the measurements at room temperature and replaced by Kapton foil (20 μm) for the measurements above RT. Diffraction signals from a silver behenate standard sample were used for *q*-scale calibration. Datasqueeze Software (version 2.1.2) was used to integrate all the two-dimensional data for the SAXD measurements.[1,2] WAXD experiments were performed at the DUBBLE beam-line (BM26B) at the European Synchrotron radiation facility (ESRF) in Grenoble, France. The 2D WAXD images were recorded using a CCD camera detector equipped with a Kodak KAI-11000 sensor. A 2 × 2 binning mode was used to acquire the images. The effective pixel size is 40.2 × 40.2 μm^2, with the actual size of the detector being 53.4 × 79.4 mm^2. The X-ray beam energy was 10 keV, and the sample-to-detector distance used was ~56 mm. Temperature of the sample was controlled with a Linkam HFS 191 sample stage. Diffraction signals from an HDPE standard sample were used

for *q*-scale calibration. Corrections for dark current and detector flat field were applied on the 2D-WAXD images of samples and before transformation into corrected 1D-profiles by performing radial integration along the azimuthal angle using the FIT2D program developed by dr. Hammersley of the ESRF.[3] The WAXD intensities were corrected by subtracting a background (scattering by the empty cell) that was normalised to the acquisition time.

Quantum-chemical calculations. To model the arrangement of the cores in the superstructure of the experimentally investigated C_3-symmetrical discotic system **1a**, quantum-chemical calculations have been performed on simplified system **2** as shown in Fig. S1. In comparison with **1a**,**b** in model **2** the outer aryl substituents are replaced by hydrogens. Although X-ray diffraction measurements[4] indicate that the observed stacking pattern is only marginally affected by substituents on the peripheral benzene moieties, the presence of the aromatic units in itself may significantly influence the structure.

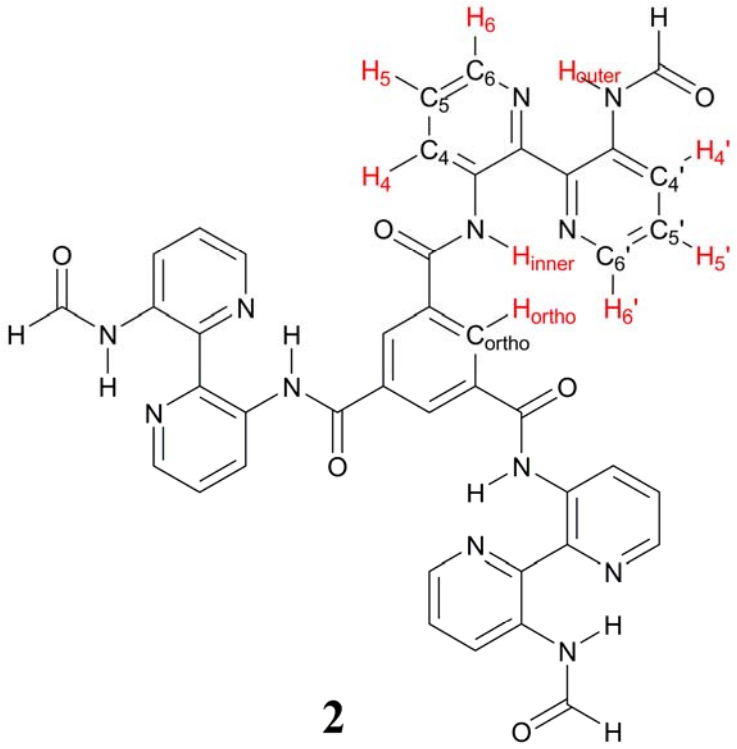

Fig. S1 Simplified C_3-symmetrical system **2** used in the quantum-chemical modelling of the helical superstructure of **1a** and **1b**.

The geometry of the monomeric species has been determined using density-functional theory (DFT) methods[5] as well as second-order Møller-Plesset perturbation theory.[6] The calculations at the DFT level have been performed using the BLYP functional[7, 8] together with a polarised split-valence (SVP) basis.[9] The same basis-set was also used in the MP2 geometry optimisation. To minimise computational efforts, all calculations have been performed within the resolution-of-identity (RI) approximation.[10, 11] To investigate the rotation of two adjacent molecules in the columnar stack of **1a**, DFT calculations (RI-DFT-BLYP/SVP) have been performed for dimers of **2** for a series of different rotation angles φ. Trimers and higher aggregates were not considered for reasons of computational costs. The geometries adopted in these single-point energy calculations are based on the optimised monomer geometries (as obtained in the DFT calculations) together with an assumed distance of 3.5 Å between the discs (in agreement with corresponding X-ray scattering results[4]). The optimal twisting angle is then obtained via energy minimisation. In order to connect the theoretical investigation of **2** with experiment, NMR chemical shifts have been computed for different oligomers of **2** based on the optimised geometries and the determined twisting angle. For the monomer and trimer of **2**, these calculations have been performed at the DFT level using the B3LYP hybrid functional[12] and the SVP basis. Additional calculations for up to pentameric stacks have been performed at the Hartree-Fock (HF) level[13] and the smaller 3-21G basis[14] in order to investigate the convergence of the computed NMR chemical shifts with stacking size and in this way to ensure a proper comparison of the theoretical results with the corresponding solid-state NMR data. All NMR chemical shift calculations have been performed using gauge-including atomic orbitals (GIAOs)[15-17] in order to ensure gauge-origin independence of the results and with TMS as reference compound for the calculation of relative NMR chemical shifts (^{1}H: 31.12 ppm (DFT-B3LYP/SVP), 33.08 ppm (HF/3-21g); ^{13}C: 187.26 ppm (DFT-B3LYP/SVP)). Finally, it should be noted that the used combinations of method,

functional, and basis set have been extensively tested with respect to their applicability. In these test calculations on a small hydrogen-bonded system, results obtained for different functionals and basis sets have been compared to more reliable MP2 data. These comparisons indicate that, for example, the overall accuracy of our theoretical results for ^{1}H-NMR chemical shifts is about 0.5 ppm.[18] All calculations have been performed with the TURBOMOLE program package.[19]

NMR spectroscopic investigations. Solid state NMR experiments were carried out on a BRUKER Advance type spectrometer operating at Larmor frequencies of 700.13 MHz and 176.06 MHz for ^{1}H and ^{13}C, respectively. To enhance spectral resolution magic angle spinning (MAS) was applied at 30 kHz with bearing gas at ambient temperature. RF pulses were applied at a transverse B1 field of 100 kHz, corresponding to a $\pi/2$ pulse width of 2.5 μs. Two dimensional ^{1}H-^{1}H double quantum (DQ) spectra were recorded using the back-to-back pulse sequence.[20, 21] The DQ coherences evolve according to the sum of the chemical shifts of the two protons involved in the coherence. WATERGATE peak suppression[22] was utilised to overcome the problem of phase distortions arising from the huge alkyl peak. ^{1}H-^{13}C correlation spectra were carried out with excitation and reconversion time of one rotor period with the REPT HSQC pulse sequence.[23] Solution ^{1}H-NMR and ^{13}C-NMR spectra of compound **1c** were recorded on a Bruker AM-400 (400.13 MHz for ^{1}H-NMR and 100.62 for ^{13}C-NMR) using tetramethylsilane as the internal reference.

Optical spectroscopy. The solvent for CD spectroscopy, methylcyclohexane, was obtained from Aldrich in spectrophotometric grade (99%) and used as received. Circular dichroism measurements were performed on a Jasco J-815 spectropolarimeter where the sensitivity, time constant and scan rate were chosen appropriately. Corresponding temperature-dependent measurements were performed with a PFD-425S/15 Peltier-type temperature controller with

a temperature range of 263-383 K and adjustable temperature slope. A cooling rate of –1 K/min was applied to ensure that the self-assembly was under thermodynamic control. For this cooling rate no hysteresis was observed when heating the solution again. In all experiments the linear dichroism was also measured and in all cases no linear dichroism was observed.

Modelling of the temperature-dependent CD data. The temperature-dependent CD-spectroscopy data were normalised by dividing the molar circular dichroism, $\Delta\varepsilon$, by the maximum molar circular dichroism, measured at low temperatures, yielding the degree of aggregation, ϕ_n, as a function of temperature:

$$\phi_n(T) = \frac{\Delta\varepsilon(T)}{\Delta\varepsilon_{MAX}}$$

The average stack length, N_n, as a function of temperature, was calculated from the degree of aggregation using the following equation, which is valid for isodesmic self-assembly.[24]

$$N_n(T) = \frac{1}{\sqrt{1-\phi_n(T)}}$$

2: X-ray data of compounds **1a,b**

Table S1 X–ray results for the mesophases of molecules under study **1a** and **1b**.

Compd.	*T* [ºC]	Phase[a]	*h k l*	d_{obs} [Å][b]	d_{calcd} [Å]	Lattice constants [Å]
1a	20	Col_{ro}	1 1 0	32.7	32.7	*a* = 65.0
			2 1 1	17.7	17.7	*b* = 37.9
			3 0 1	16.1	16.5	*p* = 25.5
			3 1 1	15.1	15.1	*h* = 3.4
			3 2 1	12.6	12.4	
			1 3 1	11.1	11.1	
			Alkyl	4.5		
				3.7		
			π-π	3.4		
1b	20	Col_{ro}	1 1 0	34.7	34.7	*a* = 68.8
			2 1 1	20.4	20.2	*b* = 40.2
			3 0 1	18.3	18.6	*p* = 31.8
			3 1 1	16.9	16.9	*h* = 3.4
			3 2 1	13.7	13.7	
			1 3 0	13.1	13.2	
			1 3 1	12.2	12.2	
			1 5 0, 1 5 1	7.9	8.0, 7.8	
			Alkyl	4.5 (br.)		
				3.7		
			π-π	3.4		
	120	Col_{ro}	1 1 0	34.7	34.7	*a* = 68.8
			2 1 1	20.1	20.2	*b* = 40.2
			3 0 1	18.3	18.6	*p* = 31.8
			3 1 1	16.9	16.9	*h* = 3.4
			3 2 1	13.8	13.7	
			1 3 0	13.1	13.2	
			1 3 1	12.3	12.2	
			1 5 0, 1 5 1	7.8	8.0, 7.8	
			Alkyl	4.5 (br.)		
				3.7		
			π-π	3.4		

[a] Col_{ro} = ordered columnar rectangular phase. [b] br. = broad maximum. [c] *h* =inter-disc distance from WAXD. *p* = distance along one column for a 120º-turn of the helix.

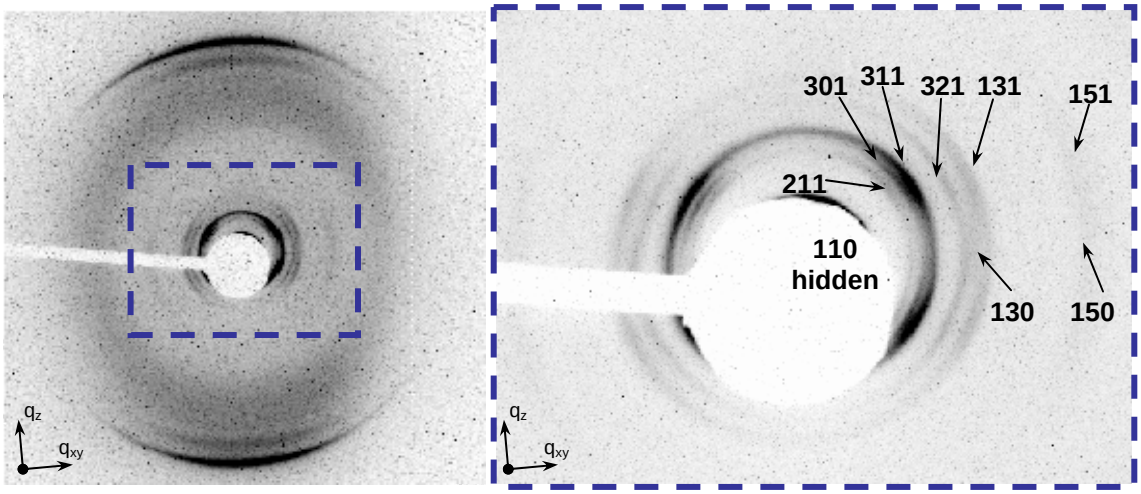

Fig. S2 left. Wide angle X-ray diffraction pattern of **1b** at 120 ºC (Fig. 2a in main text) and, right, amplification of the small angle region.

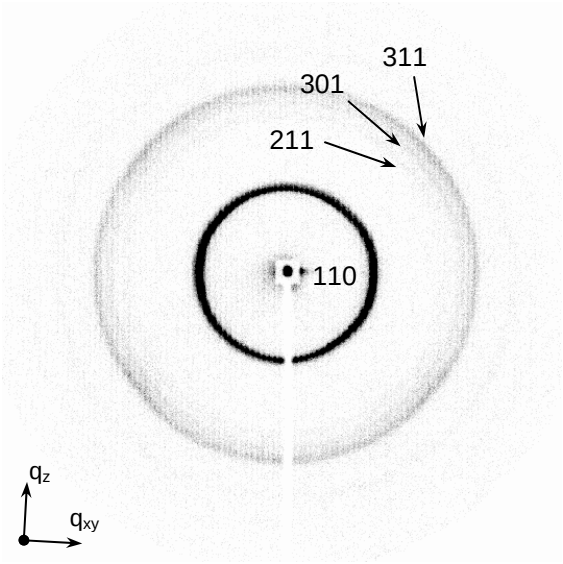

Fig. S3 Small angle X-ray diffraction pattern of **1a** at 130 ºC.

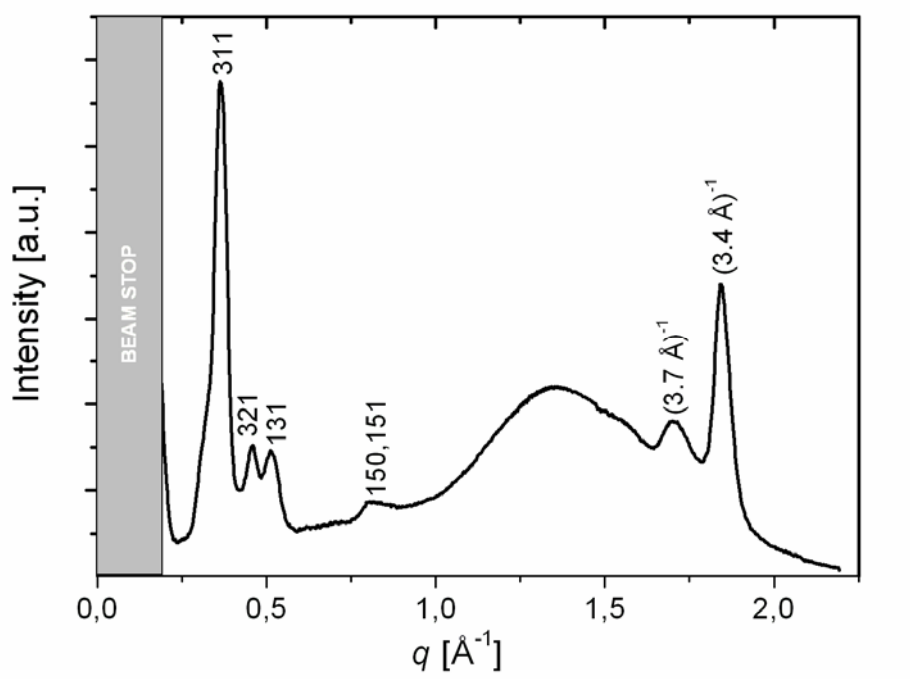

Figure S4. *q* plot of the wide angle X-ray diffraction pattern in Figure 2a (and Figure S2). Reflections 211 and 301 appear as a shoulder on reflection 311. Reflection 130 is hidden below reflections 321 and 131.

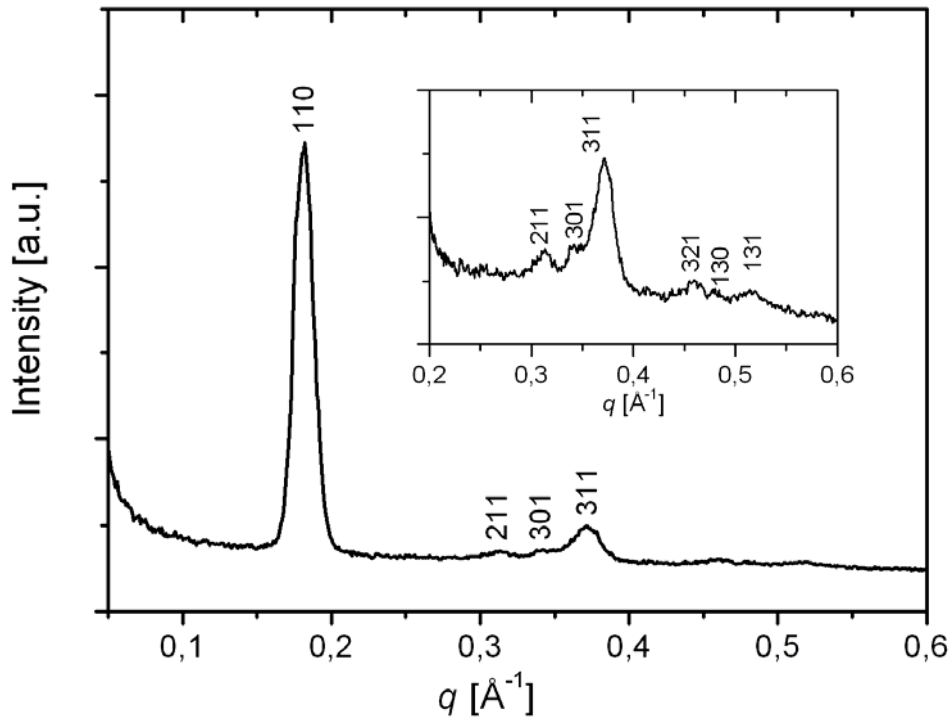

Figure S5. *q* plot of the small angle X-ray diffraction pattern in Figure 2b.

3: Variable concentration/temperature solution ^{1}H-NMR data of **1c**

Table S2 Dependence of the chemical shifts of compound **1c** in $CDCl_3$ on the concentration measured with ^{1}H-NMR (T = 298 K, Bruker 400 MHz)

c (mM)	**δ NH_{in} (ppm)**	**δ NH_{out} (ppm)**	**δ H_{ortho} (ppm)**	**δ H_4 (ppm)**	**δ H_5/ $H_{5'}$ (ppm)**	**δ H_6 (ppm)**	**δ $H_{4'}$ (ppm)**	**δ $H_{6'}$ (ppm)**
31.1	15.08	14.15	8.50	9.18	7.20/7.01	7.96	9.13	8.78
16.5	15.29	14.27	8.82	9.35	7.35/7.23	8.16	9.28	8.92
8.25	15.45	14.36	9.12	9.52	7.49/7.44	8.35	9.37	9.01
4.77	15.47	14.36	9.15	9.54	7.50/7.45	8.38	9.38	9.02
1.55	15.51	14.38	9.25	9.58	7.52	8.44	9.40	9.03

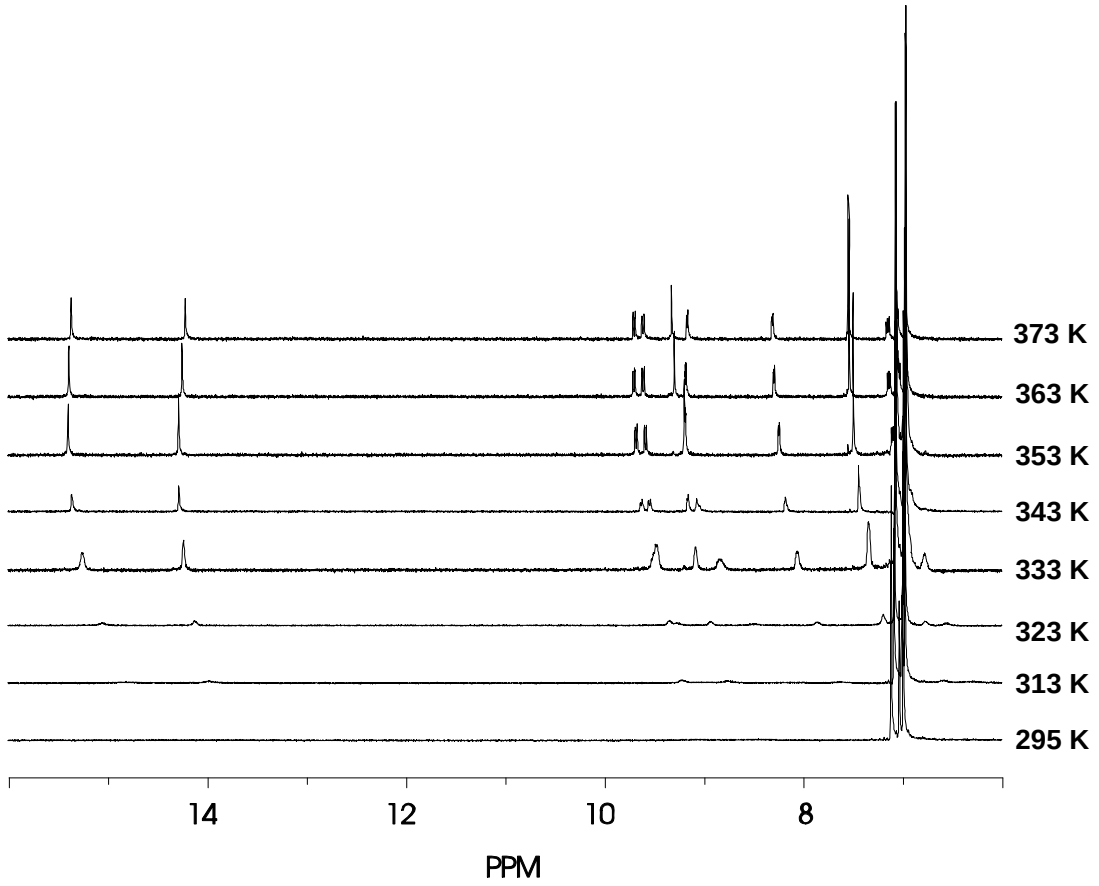

Fig. S6 Variable temperature ^{1}H NMR data of compound **1c** in toluene-*d8*.

4. References

1. http://www.datasqueezesoftware.com/index.html
2. A. P. Hammersley, S. O. Svensson, M. Hanfland, A. N. Fitch and D. Hausermann, *High Pressure Res.*, 1996, **14**, 235 - 248.
3. http://www.esrf.eu/computing/scientific/FIT2D/index.html
4. A. R. A. Palmans, J. A. J. M. Vekemans, H. Fischer, R. A. Hikmet and E. W. Meijer, *Chem. Eur. J.*, 1997, **3**, 300-307.
5. R. G. Parr and W. Yang, *Density Functional Theory of Atoms and Molecules*, Oxford University Press, New York, 1989.
6. C. Møller and M. S. Plesset, *Phys. Rev.*, 1934, **46**, 618.
7. C. Lee, W. Yang and R. G. Parr, *Phys. Rev. B*, 1988, **37**, 785.
8. A. D. Becke, *Phys. Rev. A*, 1988, **38**, 3098.
9. A. Schäfer, H. Horn and R. Ahlrichs, *J. Chem. Phys.*, 1992, **97**, 2571-2577.
10. F. Weigend, M. Häser, H. Patzelt and R. Ahlrichs, *Chem. Phys. Lett.*, 1998, **294**, 143-152.
11. K. Eichkorn, O. Treutler, H. Öhm, M. Häser and R. Ahlrichs, *Chem. Phys. Lett.*, 1995, **242**, 652-660.
12. A. D. Becke, *J. Chem. Phys.*, 1993, **98**, 5648-5652.
13. A. Szabo and N. S. Ostlund, *Modern Quantum Chemistry*, Dover Publications, New York, 1996.
14. J. S. Binkley, J. A. Pople and W. J. Hehre, *J. Am. Chem. Soc.*, 1980, **102**, 939-947.
15. R. Ditchfield, *Molecular Physics: An International Journal at the Interface Between Chemistry and Physics*, 1974, **27**, 789 - 807.
16. F. London, *J. Phys. Radium*, 1937, **8**, 397-409.
17. K. Wolinski, J. F. Hinton and P. Pulay, *J. Am. Chem. Soc.*, 1990, **112**, 8251-8260.
18. T. Metzroth, PhD Thesis, Universitaet Mainz (Germany, 2006
19. http://turbomole.com
20. M. Feike, D. E. Demco, R. Graf, J. Gottwald, S. Hafner and H. W. Spiess, *Journal of Magnetic Resonance, Series A*, 1996, **122**, 214-221.
21. I. Schnell and H. W. Spiess, *J. Magn. Reson.*, 2001, **151**, 153-227.
22. I. Fischbach, K. Thieme, A. Hoffmann, M. Hehn and I. Schnell, *J. Magn. Reson.*, 2003, **165**, 102-115.
23. K. Saalwächter, R. Graf and H. W. Spiess, *J. Magn. Reson.*, 2001, **148**, 398-418.
24. M. M. J. Smulders, M. M. L. Nieuwenhuizen, T. F. A. de Greef, P. van der Schoot, A. P. H. J. Schenning and E. W. Meijer, *Chem. Eur. J.*, 2010, **16**, 362-367.